Instrument Science Report WFC3 2010-12

Proposal 11913-IR Filter Wedge Check

E. Sabbi, J. MacKenty, T. Borders
August 24, 2010

ABSTRACT

Variations in the thickness of a filter alter the path of the incoming light beam, causing an apparent displacement of the observed sources. Proposal 11913 was designed to verify the coplanarity of the WFC3/IR filters, i.e. whether any of them was wedged, and if so, to evaluate the impact on the astrometry. We found that, with the exception of the F098M and F126N filters, the positions of stars observed through different filters, without moving the telescope, differ on average by less then 0.14 ±0.06 pixels and match the CEI specifications. In addition we found that the positional shifts increase along the X-axis and decrease along the Y-axis as a function of wavelength. The observed shifts are consistent with the fact that the refractive corrector plate (RCP) is tilted ~8.6 degree to the center of the field center chief ray.

1. Introduction

The Wide Filed Camera 3 (WFC3), that has replaced the Wide Field Planetary Camera 2 (WFPC2) on board of the *Hubble Space Telescope* (HST) during Servicing Mission 4 (SM4), features two independent channels, one operating in the wavelength range 200-1000 nm (the UVIS channel), and the other sensitive to the 800-1700 wavelength range (the IR channel). In particular WFC3/UVIS is equipped with 62 among wide-, medium-, and narrow-band filters, plus one low-dispersion grism, while WFC3/IR has 15 wide-, medium-, and narrow-band filters, 2 grisms, and an opaque element.

Variations in the thickness of a filter modify the distribution of the light beam. As a consequence, astronomical sources observed without moving the telescope through two filters of the same instrument will have different positions on the detector. If the two faces of a filter are not coplanar (or if the filter is wedged) the displacement of the light beam will cause a rigid shift of the entire field of view.

During Cycle 17 we executed two twin calibration programs (11913 and 11923; P.I. Mackenty) to measure the relative displacement, caused by filter wedge, of the stars in the cluster NGC 1850 in each of the IR and UVIS filter respectively. We report the results obtained for the IR channel using the data acquir-

Operated by the Association of Universities for Research in Astronomy, Inc., for the National Aeronautic and Space Administration.

ed in proposal 11913: in Section 2 we present the data, while the analysis is described in Section 3, results and conclusions are presented in Section 4. Results for the UVIS tests will be presented in a forthcoming ISR (Borders et al. 2010).

2. Data

The IR channel is equipped with five broad-band filters (F105W, F110W, F125W, F140W, and F160W), four medium-band filters (F098M, F127M, F139M, and F153M), and six narrow-band filters (F126N, F128N, F130N, F132N, F164N, and F167N), plus two low-dispersion grisms (G102 and G140). Filters and grisms are housed in an eighteen slots wheel, called Filter Select Mechanism (FSM), with the 18th slot reserved to the opaque element called BLANK. When an IR observation is commanded, the selected filter is rotated into the light beam, and since the FSM can rotate in both the directions in the IR channel, it always takes the shortest path to put the filter in place. Figure 1 (from the Wide Field Camera 3 Instrument Handbook Cycle 18) shows how the filters are housed in the FSM. The first household on the right side of the BLANK element has been defined as position 1 of the FSM, and hosts to the F160W filter, while filter F164N is in position 17.

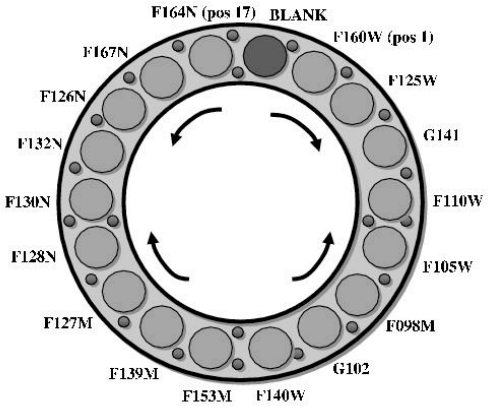

Figure 1: IR filter wheel, from the Wide Filed Camera 3 Instrument Handbook Cycle 18. The postions of the filters, grisms and of the BLANK are shown. The rotation directions are indicated by the curved arrows.

To check if any of the WFC3/IR filters are affected by wedge, we observed the young and bright star cluster NGC 1850 in the Large Magellanic Cloud with each filter. This cluster was chosen because it has a low amount of extinction and hosts several bright red and blue stars, which make it a good target for both the IR and UVIS tests.

For the WFC3/IR analysis, we acquired one short exposure for each filter using the MULTIACCUM mode. To minimize shifts between consecutive observations due, for example, by the guide star (re) acquisition, all the images were acquired within the same orbit. Finally to minimize the read-out overheads all data were acquired using a default 512 x 512 sub-array. IR data of NGC 1850 were acquired starting from the F105W filter (corresponding to position 5 in Figure 1) and then clockwise rotating the FSM toward the F125W filter. We acquired an extra F105W image at the end of the orbit to verify the constant tracking of the telescope during the observations (i.e. because it lost the Guide Star). Table 1 reports the log of the observations.

IMAGE NAME	FILTER	STEP	NSAMP	Total Exp. Time (sec)
ibcg01fiq	F105W	RAPID	6	17.549
ibcg01fhq	F098M	RAPID	6	17.549
ibcg01fwq	F140W	RAPID	6	17.549
ibcg01fvq	F153M	RAPID	8	23.458
ibcg01fqq	F139M	RAPID	8	23.458
ibcg01fmq	F127M	RAPID	6	17.549
ibcg01fnq	F128N	RAPID	10	29.323
ibcg01foq	F130N	RAPID	10	29.323
ibcg01fpq	F132N	RAPID	10	29.323
ibcg01flq	F126N	RAPID	10	29.323
ibcg01fjq	F167N	RAPID	10	29.323
ibcg01fkq	F164N	RAPID	10	29.323
ibcg01fuq	F160W	RAPID	7	20.526
ibcg01ftq	F125W	RAPID	6	17.549
ibcg01frq	F110W	RAPID	6	17.549
ibcg01fxq	F105W	RAPID	6	17.549

Table 1: Log of the observations for proposal 11913. The file name is listed in the 1st column, while column 2 reports the filter selected to acquire the data. All the data were acquired using the RAPID read mode, as shown in column 3, with the number of samplings listed in column 4. The 5th column reports the total exposure time in seconds. Data were acquired on February 6th, 2010.

3. Analysis

The data-set was retrieved from the Multimission Archive at Space Telescope (MAST) and re-processed with the 1.7 version of the calibration pipeline CALWF3 using the most up-to-date versions of bias and dark files. As part of the default calibration, in the IR, the pipeline applies an “up-to-the-ramp” fit through the non destructive reads to remove the cosmic rays and recover the information associated with saturated stars, and finally converts the images from counts to count rates (refer to Appendix E of the Wide Filed Camera 3 Instrument Handbook for a detailed description of the calibration steps performed by CALWF3). An atlas of

the images used in this analysis is shown in Appendix A.

For each image the position of the stars was measured using DAOPHOT in IRAF. In each image the sources were identified using the routine DAOFIND, and then aperture photometry using PHOT was performed.

To refine the position of the detected sources for each image we made an empirical PSF, by selecting ~10 well isolated stars, and then we ran ALLSTAR to perform PSF-fitting on each image. This also allowed us to discard non-stellar objects such as cosmic rays (CRs) and hot pixels that were not removed by CALWF3, or galaxies and blended stars. To do this we used two of the statistical parameters provided by ALLSTAR to evaluate how much a detected source is close to the empirical PSF. In particular we used the χ^2 of the residual, and retained only those sources with χ^2 <1.5, and the sharpness parameter to discard those objects that were either too sharp (sharpness<-0.2) or too broad (sharp>0.2) to be a star.

Individual stars were identified and matched in all available catalogs and we computed the positional X and Y shifts of each object with respect to the reference image (ibcg01fiq_flt.fits) in the F105W filter (see Table 1). A 3σ-clipping rejection was used to reject possible incorrect object matching caused by the different crowding that characterize the various images (see Appendix A). The difference along the X and Y directions are shown in Figures 2, 3, 4, and 5. With the exception of the F098M, and F126N filters where the shifts with respect of the reference image is more than 0.3 ± 0.03 pixels, the average shift is 0.14 and the standard deviation is 0.06 pixels. For each filter average shifts are listed in Table 2.

To verify if there is any wavelength dependence, we examined the shifts along the Y axes (Figure 6 - *upper panel*), the X axes (Figure 6 - *middle panel*) and the total shifts (Figure 6 - *lower panel*) as a function of wavelength. We did not find any obvious relation between the total shift and the wavelength (Figure 6 - *lower panel*). We found a moderate dependences with wavelength along both the X and Y axes, consistent with the tilted angle of about 8.6° between the RCP (which applies the spherical-aberration correction) and the field center chief ray.

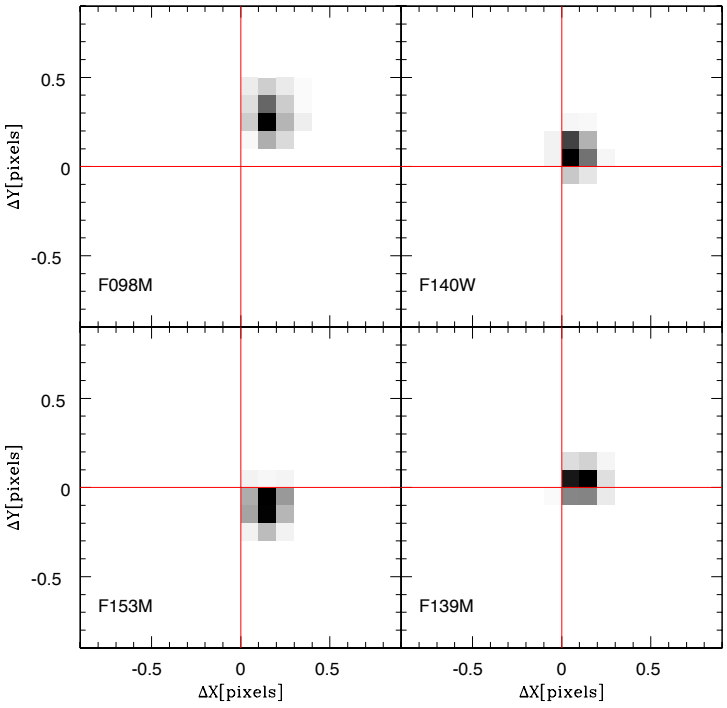

Figure 2: Difference between the position of the stars in the images acquired with the F098M, F140W, F153M and F139M filters, and the position on the reference image in the F105W filter. The red lines highlight the 0,0 (no shift) position.

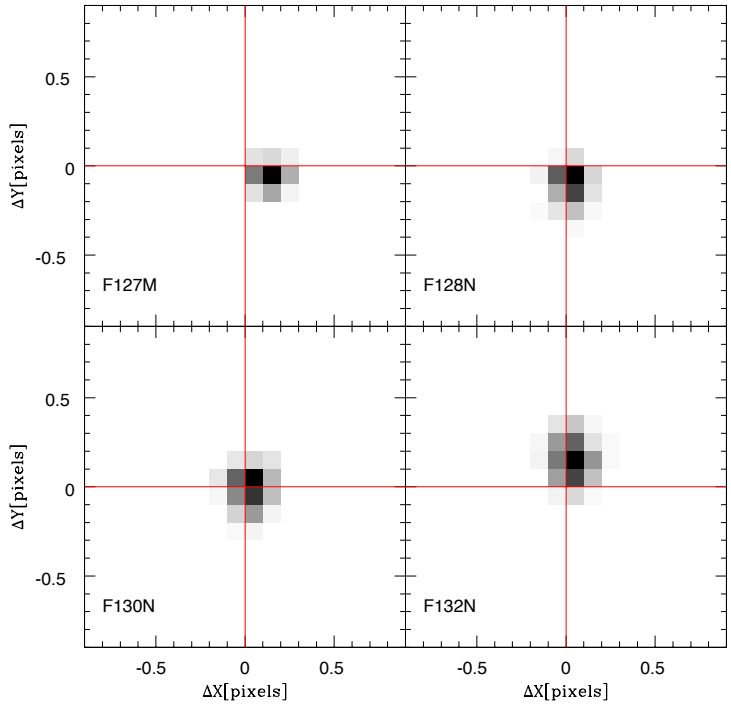

Figure 3: Same as Figure 2, but for the filters F127M, F128N, F130N and F132N.

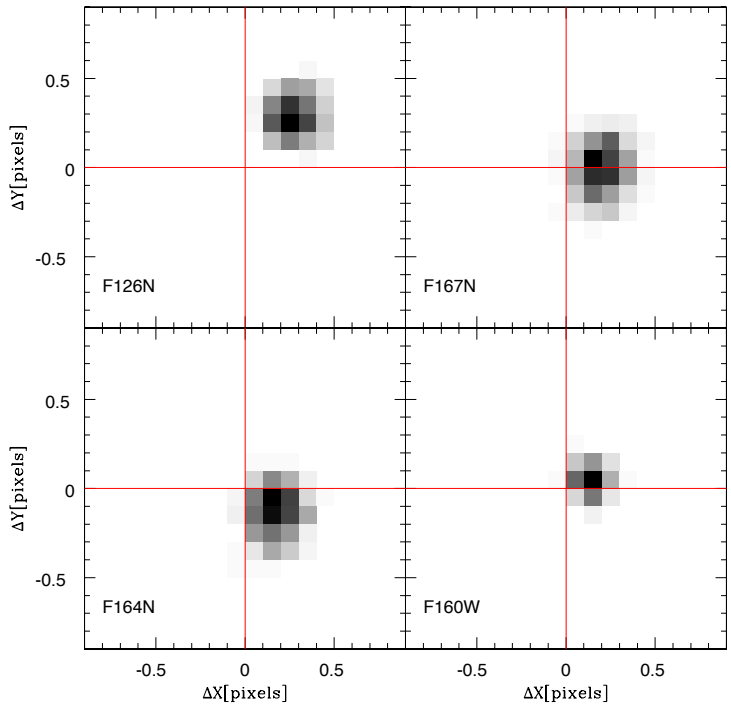

Figure 4: Same as Figure 2, but for the filters F126N, F167N, F164N and F160W.

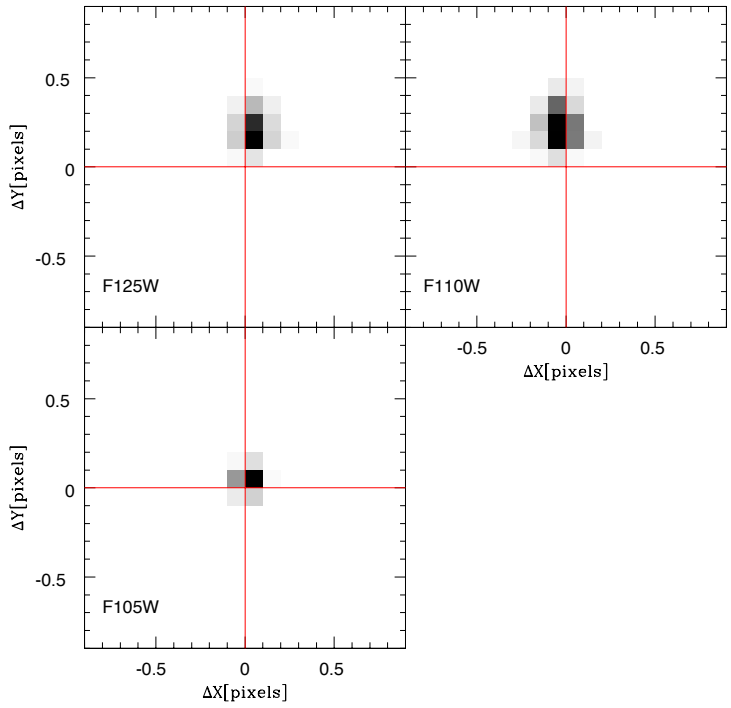

Figure 5: Same as Figure 2, but for the filters F125W, F110W, and F105W.

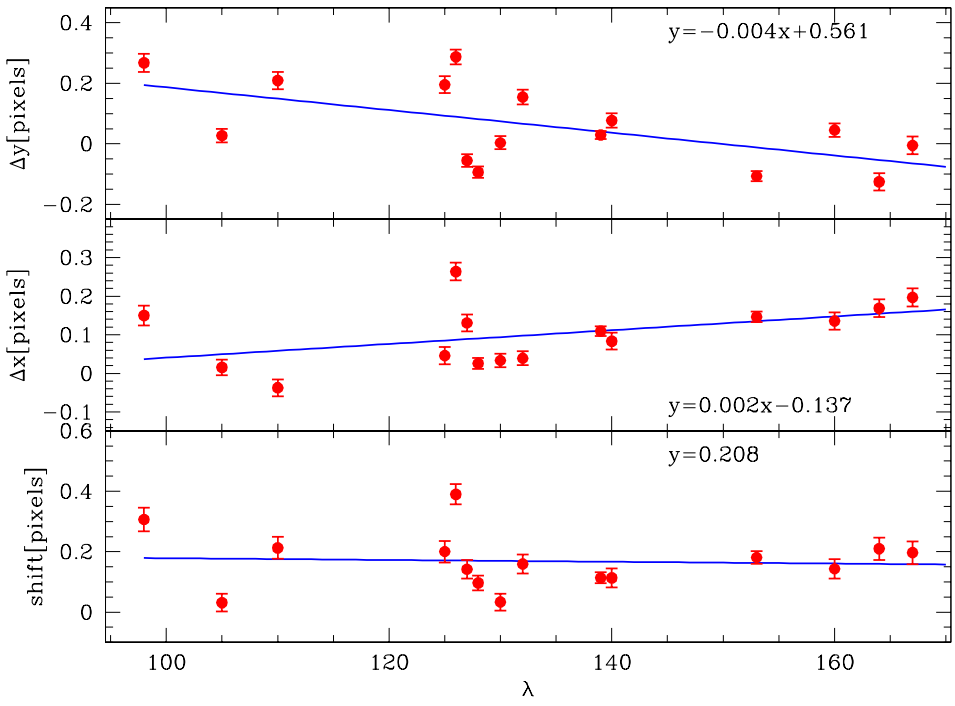

Figure 6: Average shifts of the stars measured in each image with respect to the reference image in the F105W filter as a function of wavelength along the Y-axes (upper panel), X-axes (middle panel) and total shift (lower panel). In each panel the blue line represents the least square fit. The equation that provide the best fit is shown in each panel.

FILTER	Δx (pixels)	Δy (pixels)	Shift (pixel)
F098M	0.150 ± 0.026	0.268 ± 0.030	0.309 ± 0.034
F140W	0.083 ± 0.020	0.077 ± 0.022	0.113 ± 0.030
F153M	0.146 ± 0.022	-0.106 ± 0.029	0.186 ± 0.036
F139M	0.110 ± 0.022	0.029 ± 0.028	0.114 ± 0.036
F127M	0.131 ± 0.023	-0.055 ± 0.024	0.143 ± 0.034
F128N	0.026 ± 0.022	-0.093 ± 0.021	0.095 ± 0.030
F130N	0.033 ± 0.014	0.004 ± 0.019	0.030 ± 0.024
F132N	0.039 ± 0.018	0.154 ± 0.022	0.155 ± 0.028
F126N	0.264 ± 0.018	0.287 ± 0.025	0.389 ± 0.031
F167N	0.196 ± 0.012	-0.005 ± 0.013	0.200 ± 0.018
F164N	0.169 ± 0.022	-0.125 ± 0.024	0.214 ± 0.032
F160W	0.136 ± 0.013	0.046 ± 0.016	0.149 ± 0.021
F125W	0.046 ± 0.022	0.195 ± 0.023	0.206 ± 0.032
F110W	-0.037 ± 0.023	0.209 ± 0.029	0.214 ± 0.037
F105W	0.015 ± 0.023	0.027 ± 0.030	0.036 ± 0.038

Table 2: Average shifts of the stars in the various filters with respect to the reference image ibcg01fiq. Filters are listed in column #1, average shifts in pixels along the abscissa are in column #2, while column 3 reports average pixel shifts measurements along the ordinate. The fourth column reports the total shifts.

4. Summary and Conclusions

During Cycle 17 we observed the young star cluster NGC 1850 (calibration proposal 11913) to verify and quantify if any of the WFC3/IR imaging filters is affected by wedge. By observing the cluster in all the WFC3/IR filters without moving the telescope we were able to directly measure the displacement of sources over the detector by one filter with the respect of another.

With the exception of the F098M and F126N filters, which show a displacement relative to the first image bigger than 0.3 pixels, the average shift for all the other filters is 0.14 ± 0.06 pixels matching the CEI specification. Kuntschner et al (ISR-WFC3 2009-17) found that the sources in images acquired through the F160W filter showed only a small offset with the respect of the F140W filter (dx=0.057; dy=-0.045). We measured the shifts along the X and Y axis of the stars detected in the F160W image with the respect of those found in the F140W image, and found dx=0.031 0.027 and dy=-0.040 0.029, confirming the previous

finding.

We also find that the displacement of the detected sources increases along the X-axis and decrease along the Y-axis as a function of wavelength. This behavior is consistent with the tilted angle of about 8.6 degrees between the RCP (which applies the spherical-aberration correction) and the field center chief ray. At the moment of writing this ISR we are not planning to insert the offsets found among the various filters in the IDCTAB used by multidrizzle to correct the geometric distortion.

Reference

Kuntschner, H, Bushouse, H., Kümmel, M., Walsh, J.R 2010, WFC3 Instrument Science Report, WFC3-2009-17, "WFC3 SMOV calibration proposal 11552: Calibration of the G141grism"

Wong, M.H., Pavlovsky, C., Long, K., et al. 2010, "Wide Field Camera 3 Instrument Handbook, Version 2.0" (Baltimore: STScI)

Appendix A

Atlas of the images acquired as part of proposal CAL 11913. Images are ordered for increasing filter wavelength, from F098M to F167N. Note the increase of the Airy ring brightness at longer wavelnegths.

Figure 7: NGC 1850 observed through the WFC3/IR F098M filter.

Figure 8: NGC 1850 observed through the WFC3/IR F105W filter.

Figure 9: NGC 1850 observed through the WFC3/IR F110W filter.

Figure 10: NGC 1850 observed through the WFC3/IR FF125W filter.

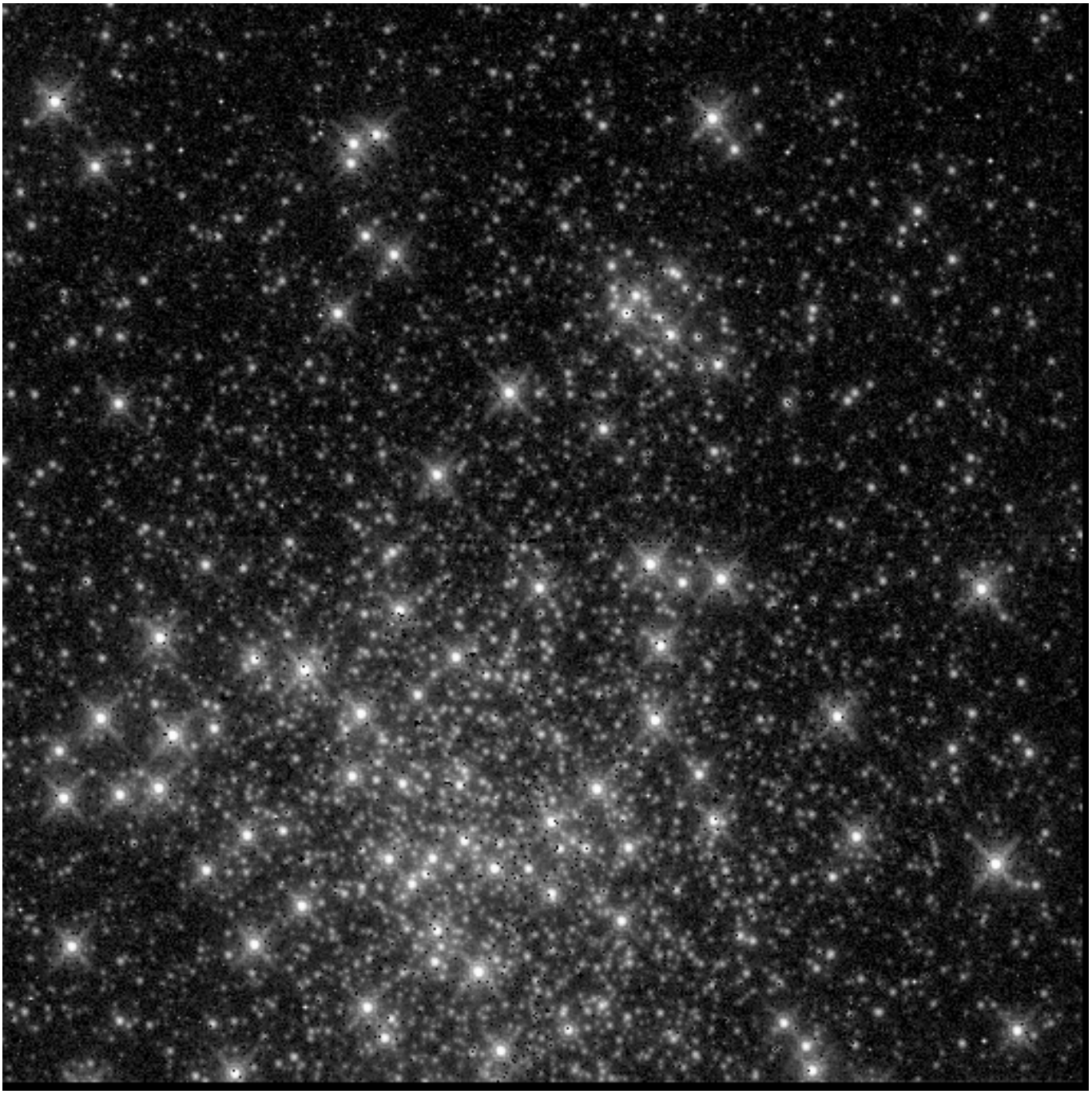

Figure 11: NGC 1850 observed through the WFC3/IR F126N filter.

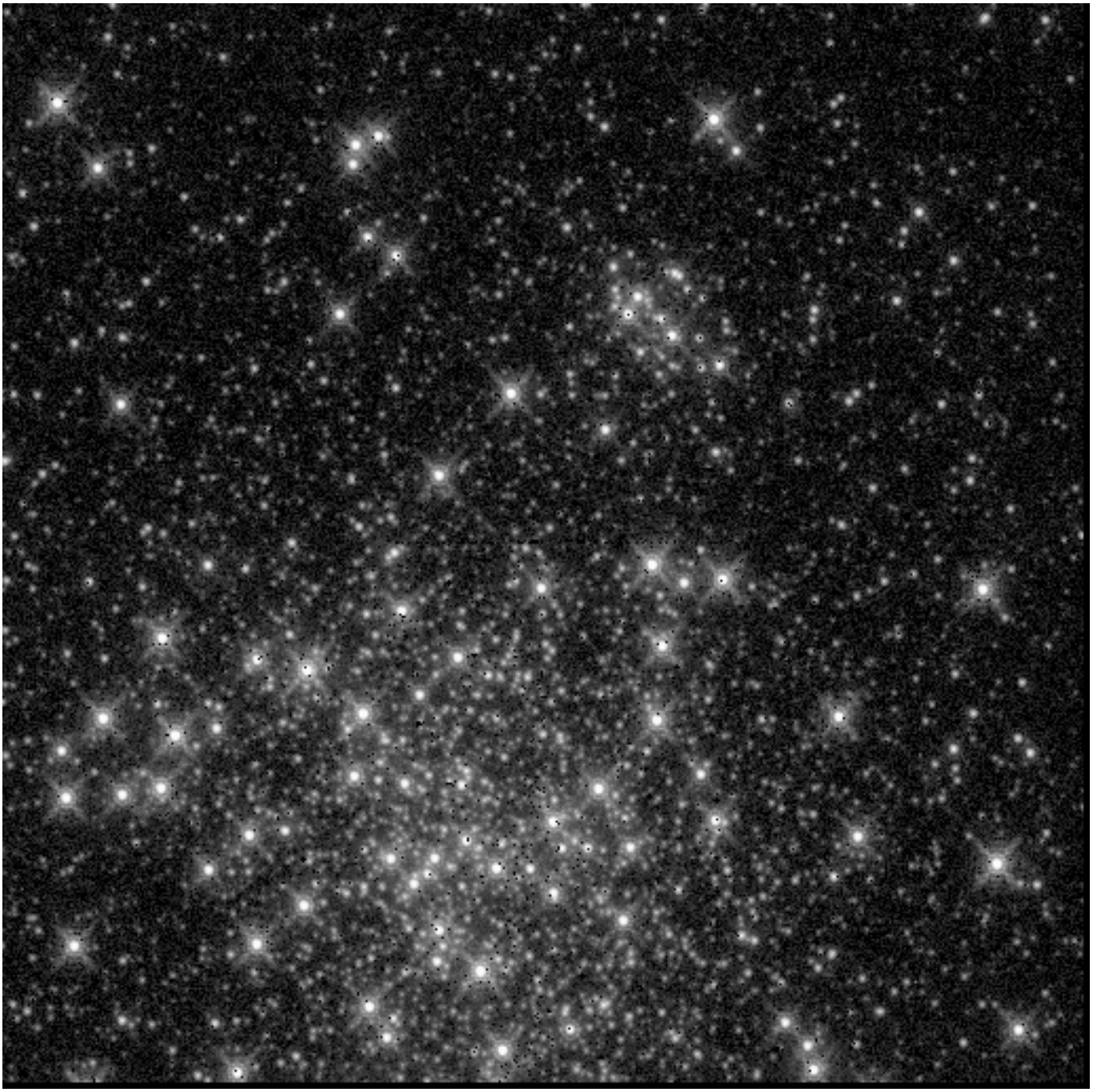

Figure 12: NGC 1850 observed through the WFC3/IR F127M filter.

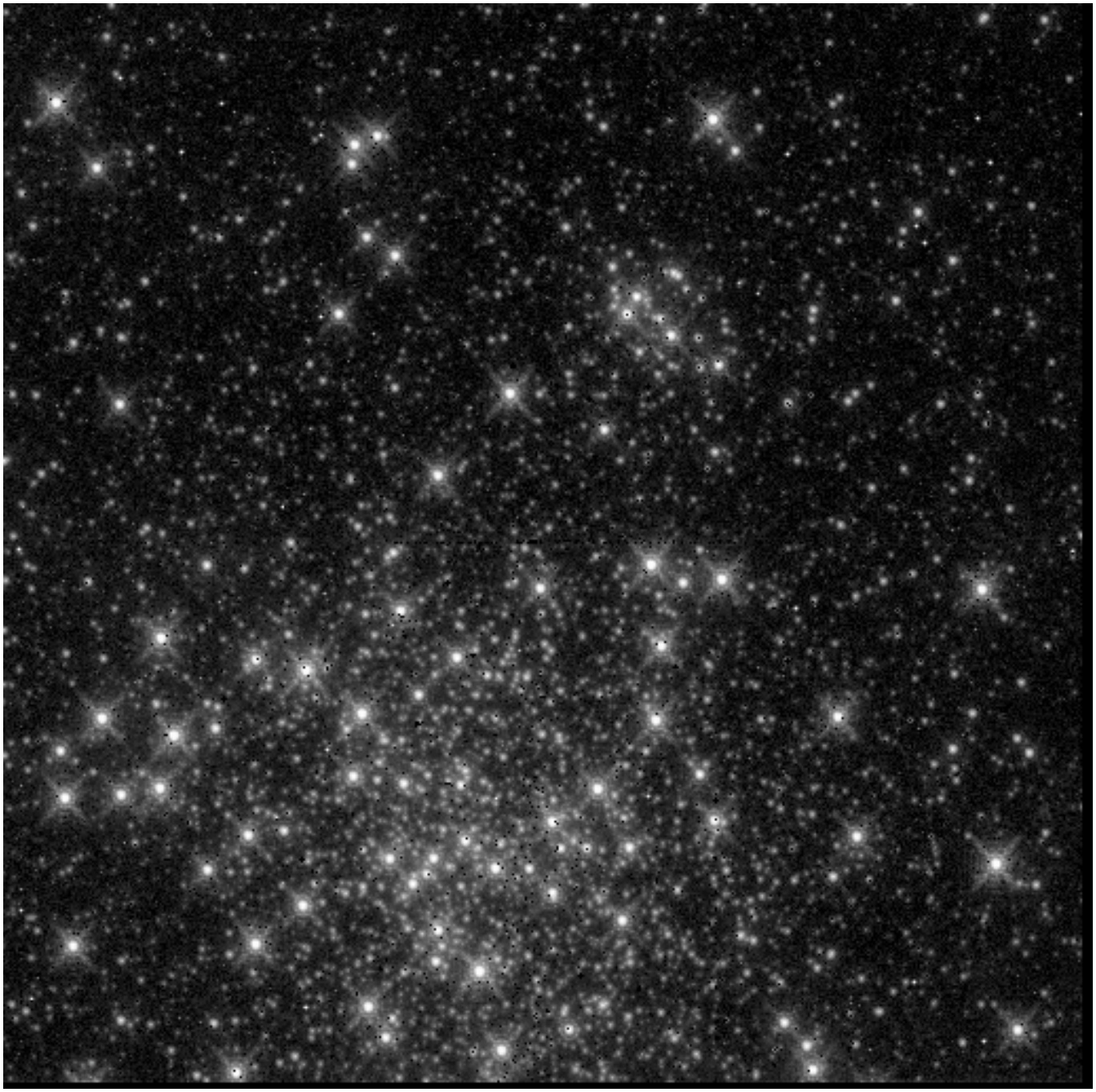

Figure 13: NGC 1850 observed through the WFC3/IR F128N filter.

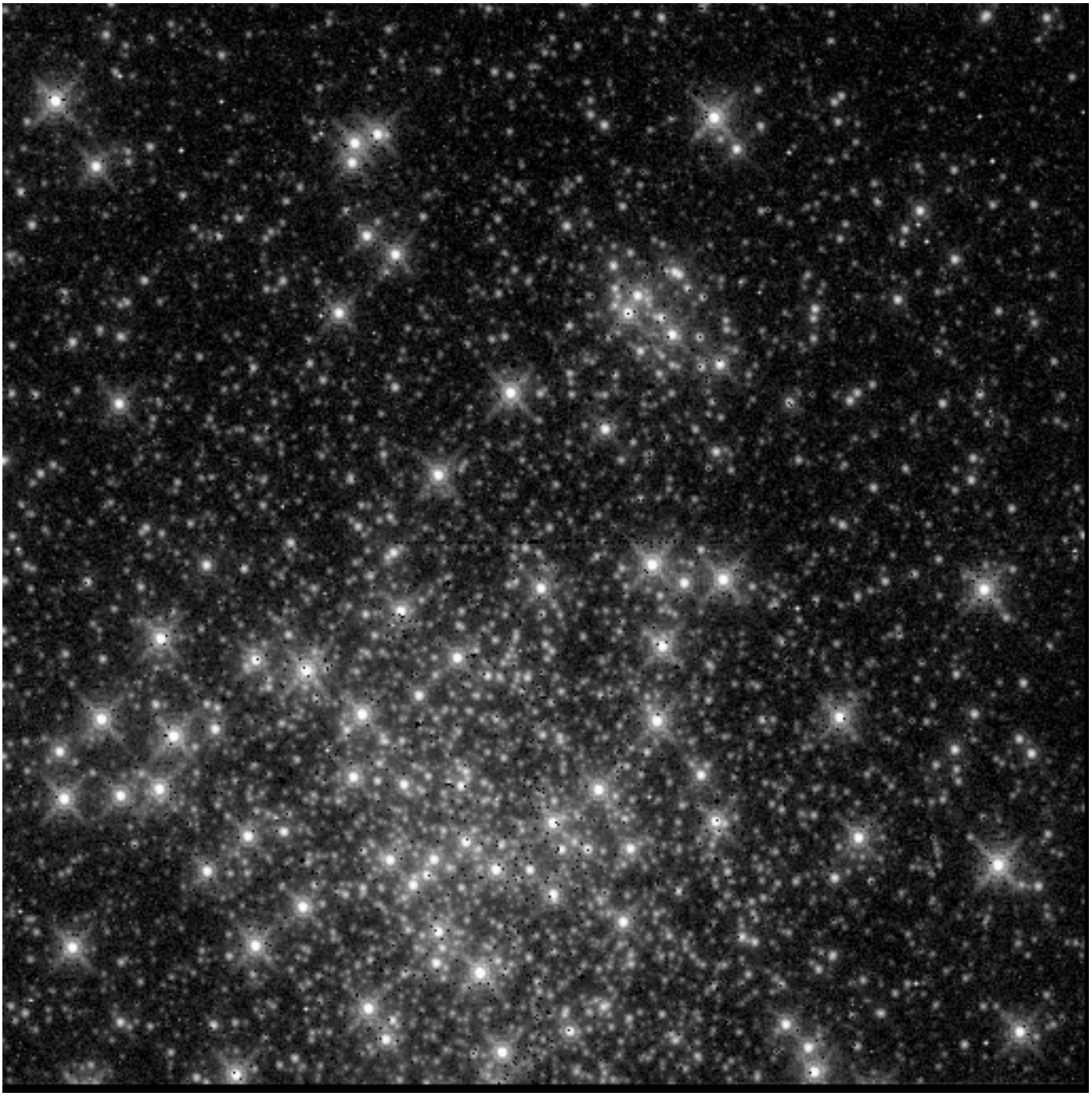

Figure 14: NGC 1850 observed through the WFC3/IR F130N filter.

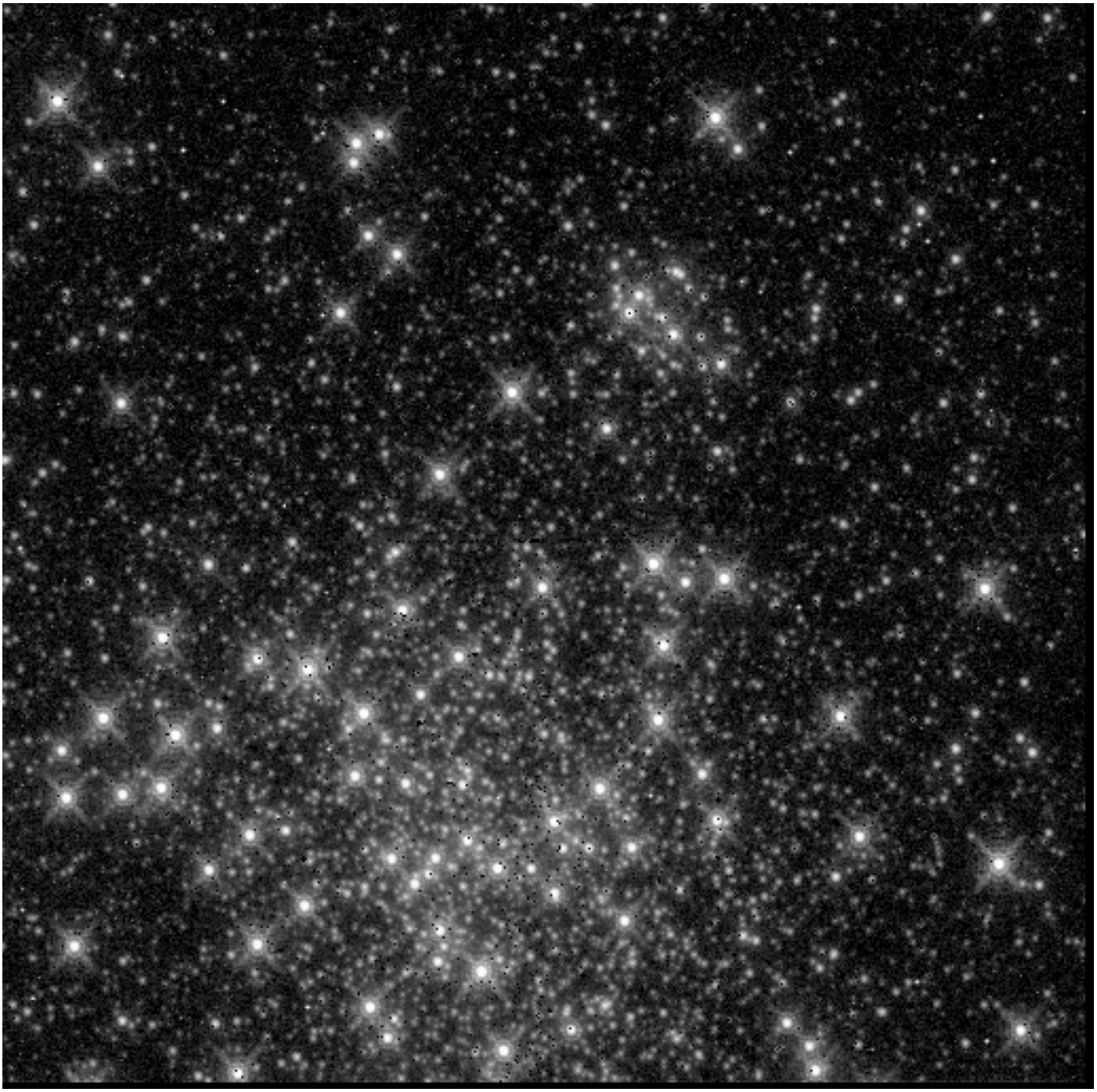

Figure 15: NGC 1850 observed through the WFC3/IR F132N filter.

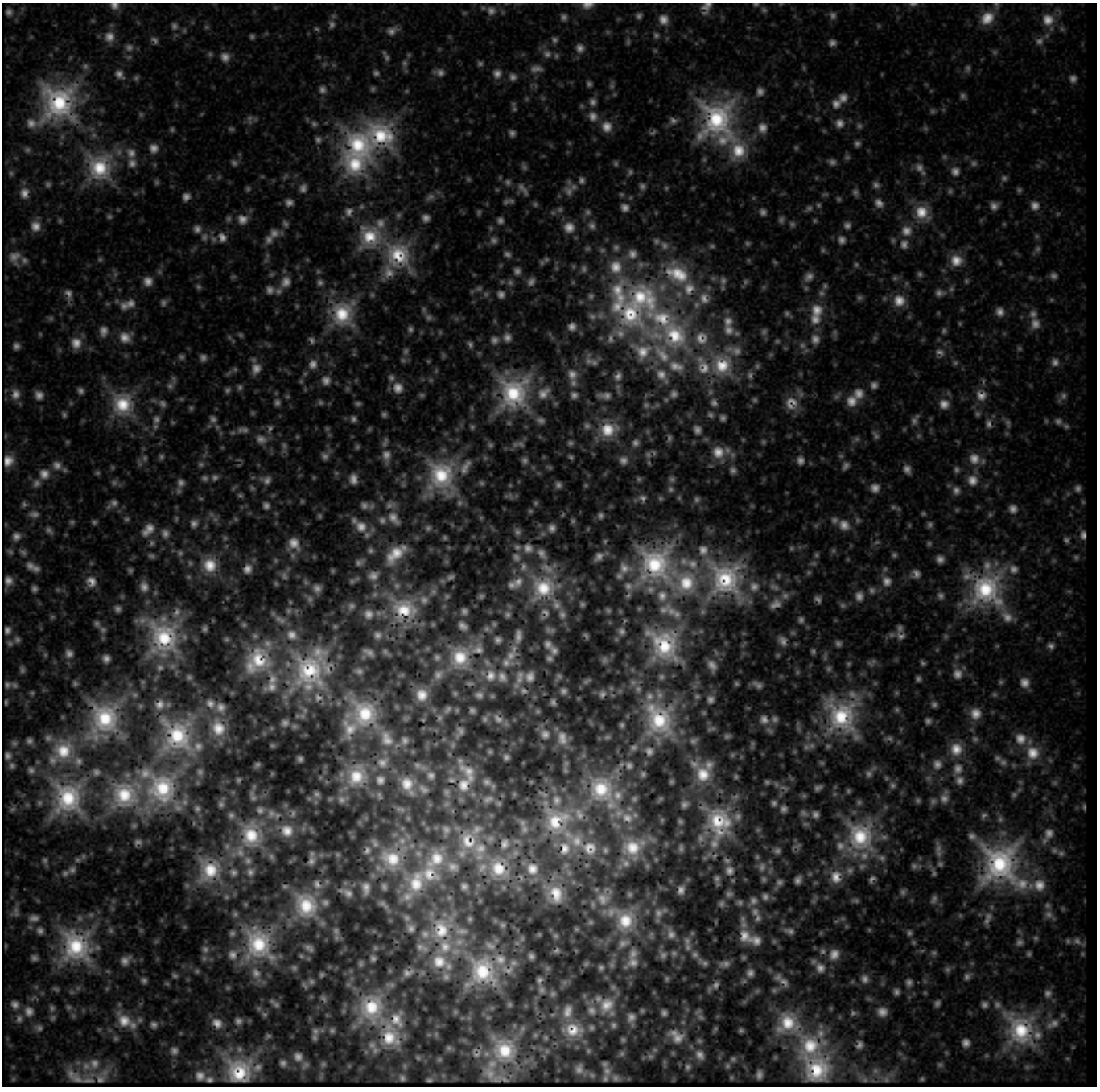

Figure 16: NGC 1850 observed through the WFC3/IR F139M filter.

Figure 17: NGC 1850 observed through the WFC3/IR F140W filter.

Figure 18: NGC 1850 observed through the WFC3/IR F153M filter.

Figure 19: NGC 1850 observed through the WFC3/IR F160W filter.

Figure 20: NGC 1850 observed through the WFC3/IR F164N filter.

Figure 21: NGC 1850 observed through the WFC3/IR F167N filter.